**Physica Status Solidi (a) 207 (2010) 1148**
http://dx.doi.org/10.1002/pssa.200983359

# Nanocrystallization kinetics under instantaneous growth approximation: experiments and cellular automata simulations

**J. S. Blázquez [*], M. Millán, C. F. Conde, and A. Conde**

Departamento de Física de la Materia Condensada, Universidad de Sevilla-ICMSE, 1065, 41080, Sevilla

**PACS** 61.46.-w, 64.70.dg, 64.60.qe, 68.55.at

* Corresponding author: e-mail jsebas@us.es, Phone: +34 954 556029, Fax: +34 954 552 870

Nanocrystallization kinetics is analyzed in the frame of instantaneous growth approximation, which implies that the time required for a crystallite to reach its final size is negligible with respect to the time required for the nanocrystallization process. This approach strongly simplifies the kinetic analysis and allows us to obtain the nucleation rate from both isothermal and non-isothermal nanocrystallization processes. Moreover, as no constraining mechanism is considered but the absence of growth, the results could be discussed in the frame of Johnson-Mehl-Avrami-Kolmogorov theory with a growth index equal to zero. Cellular automata simulations are in agreement with the observed kinetics and microstructure.

## 1 Introduction

Thermally activated nanocrystallization processes in metallic alloys consist of the formation of a partially crystalline material with 40-70 % in volume of nanocrystals embedded in a residual amorphous matrix [1]. This implies the formation of an atypically huge number of crystalline nuclei. The observed constraining in the crystal growth has been explained by the so called soft impingement [2] due to the slow diffusing atoms, which pile up at the edge of the growing crystals.

Although Jhonson-Mehl-Avrami-Kolmogorov [3-5] (JMAK) theory is widely used to describe the nanocrystallization kinetics, the values of the Avrami exponent $n$~1 are out of the values predicted by the theory: $n = n_I + D\, n_G$, with $n_I$ =1 corresponding to a constant nucleation rate, $n_I$ >1 to an increasing nucleation rate, and $n_I$ <1 to a decreasing nucleation rate, $D$ is the dimensionality of the crystal growth and $n_G$ = 1 for interface controlled growth and $n_G$ = ½ for diffusion controlled growth [6]. In fact, JMAK theory only considers the geometrical impingement between crystallites when they touch each other. It can be defined an extended crystalline fraction, $X^*$, which is the crystallized fraction in the absence of such restriction (without considering that crystal cannot growth where a crystal is already formed). This extended crystalline fraction is linked to the actual crystalline fraction as:

$$\frac{dX}{dX^*} = (1 - X) \qquad (1)$$

It is worth mentioning that the transformed fraction, $X$, at the end of the process becomes 1, but the crystalline volume fraction is lower as some amorphous matrix remains at the end of the process.

Equation 1 can be modified to consider a stronger impingement than that only due to the geometrical effect:

$$\frac{dX}{dX^*} = (1 - X)^{2-\gamma} \qquad (2)$$

where $\gamma$ is the impingement factor [7]. Other authors describe the same equation in terms of the impingement parameter $\eta$ =1/(1-$\gamma$) [8]. In any case, the values of $\gamma$ are between 0 and 1. In the case of $\gamma$=1, Eq. 1 is recovered and JMAK theory is applied. In the case of $\gamma$=0, Austin-Rickett equation is achieved [9].

A very simplistic idea could describe an initial fast growth of the crystallites till the surface of the crystal is covered by the rejected atoms non soluble in the crystal. Afterwards, the growth is very slow. If this very slow growth is neglected, the time required by the growing crystal to achieve an almost constant size becomes very small in comparison with the time required by the nanocrystallization process to be completed. Under these premises, it is possible to establish an instantaneous growth approximation [10,11], in which the crystallization kinetics is reduced to the nucleation of crystallites with a constant size.

In this work, isothermal and non-isothermal kinetics of an alloy series of composition $Fe_{78-z}Co_zNb_6B_{16-y}Cu_y$ (z=18, 39 and 60; y=0, 1) will be analyzed in the frame of instantaneous growth processes. Experimental results agree with results from cellular automata simulation.

## 2 Nanocrystalline microstructure

Figure 1 shows transmission electron images of the studied nanocrystalline alloys. 3D atom probe results show that the composition of nanocrystals is $Fe_{100-z}Co_z$, being z the Co content of the nominal composition of the alloy [12].

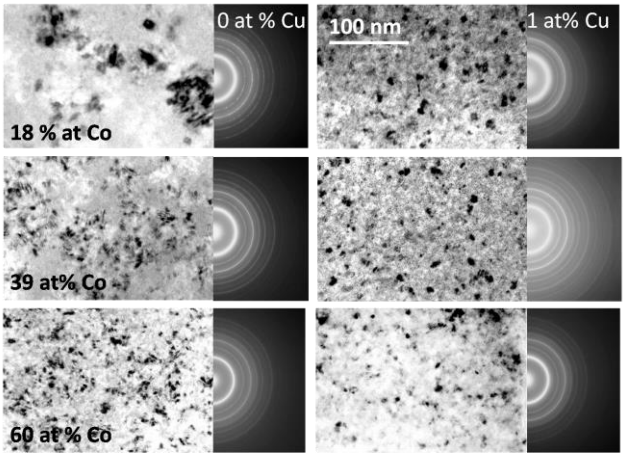


**Figure 1** Bright field TEM images and selected area diffraction patterns of the studied nanocrystalline alloys.

The developed microstructures exhibit the formation of bcc nanocrystals of ~5 nm in diameter, forming agglomerates in Cu free alloys, which size decreases as Co increases in the alloy. These dependencies can be understood as the result of the competition of two different nucleation phenomena: either in isolated regions, or in contact with an already formed crystallite. The former has the advantage of nucleating in a region rich in Fe, but the interface energy between the nucleus and the surrounding amorphous is high. In the latter nucleation phenomenon, which could be also understood as epitaxial growth, the interface energy of the new nucleus is smaller but the region might have a lower Fe concentration. The absence of agglomerates of crystallites in Cu containing alloys is due to the formation of Cu clusters [12], which reduces the interface energy of an isolated nucleus eliminating the advantage of the "in contact" nucleation. As Co content increases, the depletion in Fe in the surrounding of a crystal is enhanced and therefore, the size of the agglomerates is reduced and in the limit they are not formed at all as there is not enough Fe to form a new crystal in the neighborhood of a previous one (e.g. 60 % of Co alloy). Microstructure and orientation relationship of an agglomerate can be observed in figure 2, where a high resolution electron micrograph is shown.

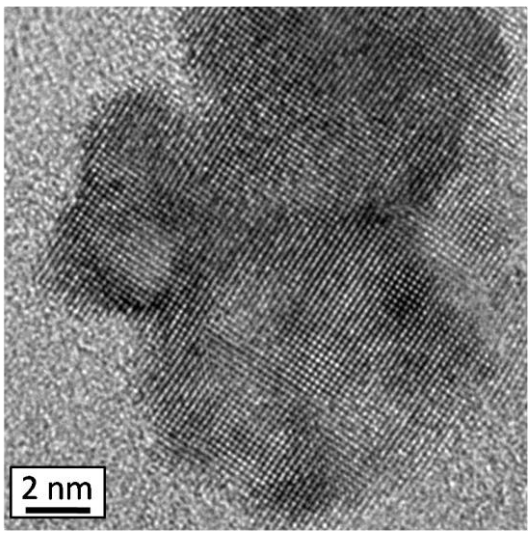

**Figure 2** High resolution TEM image showing an agglomerate in the [100] orientation for the alloy with 18 at % of Co and without Cu.

## 3 Kinetic approximations

### 3.1 JMAK extension to non-isothermal regimes

Considering the functional form of the extended crystalline fraction

$$X^{ext} = \left[K(T)\cdot\left(t-t_0\right)\right]^n \tag{3}$$

the well known expression *X(t)* for JMAK theory is found:

$$X = 1-\exp\left[-\left\{K(T)\cdot\left(t-t_0\right)\right\}^n\right] \tag{4}$$

where *K(T)* is the frequency factor, *n* is the Avrami exponent and $t_0$ is the incubation ~~induction~~ time. A local value of the Avrami exponent, *n(X)*, can also be obtained for the isothermal regimes from:

$$n(x) = \frac{d\ln\left[-\ln\left(1-X\right)\right]}{d\ln\left(t-t_0\right)} \tag{5}$$

For the non-isothermal regimes [13], taking into account the thermal dependence of *K(T)*:

$$k(T) = k_0\exp\left(-\frac{Q}{RT}\right) \tag{6}$$

the value of the local Avrami exponent can be obtained as:

$$\frac{d\ln\left[-\ln\left(1-X\right)\right]}{d\ln\left(\frac{T-T_o}{\beta}\right)} = n(X)\left\{1+\frac{d\ln\left(k\right)}{d\ln\left(\frac{T-T_o}{\beta}\right)}\right\} = \tag{7}$$

$$= n(X)\left\{1+\frac{Q}{RT}\left(1-\frac{T_o}{T}\right)\right\}$$

where $\beta$ is the heating rate, $Q$ is the effective activation energy, $R$ is the gas constant and $T_o$ is the crystallization onset temperature. This expression allows us to obtain the local Avrami exponent from a single non-isothermal scan and a raw estimation of the activation energy independently of the heating rate.

### 3.2 Instantaneous growth approximation

Assuming an instantaneous growth, the extended transformed volume fraction will be developed only due to nucleation of crystallites with a constant size $<d>$ and can be written as:

$$X^{ext} = \frac{1}{x_C}\frac{\pi<d>^3}{6}\int_0^t I(\tau)d\tau + X^{ext}(0) \tag{8}$$

where $x_C$ is the crystalline volume fraction at the end of the nanocrystallization process and $I$ is the nucleation rate. Combining equation (1) and (8), it is possible to obtain this nucleation rate as a function of the transformed fraction and the temperature:

$$I(X,T) = \frac{6x_C}{\pi<d>^3}\frac{1}{1-X}\frac{dX}{dt}(T) \tag{9}$$

Both *dX/dt* and *X* were obtained from isothermal and non-isothermal DSC scans on a Perkin-Elmer DSC7 calorimeter after normalizing using the enthalpy of the complete nanocrystallization process.

## 4 Results and discussion

### 4.1 Experiments

Figure 3 shows the local Avrami exponents obtained from non-isothermal scans at different $\beta$ for the alloy with 18 at. % of Fe and without Cu. The corresponding DSC scans are shown in the inset of the figure. The $\beta$ independency of the curves supports the isokinetic approach.

Figure 4 shows $n(X)$ exponents obtained from isothermal scans performed at different temperatures below and above the crystallization onset temperature and shown in the inset. Values corresponding to a non-isothermal regime are also shown for comparison. Both regimes agree describing a very slow kinetics, which Avrami exponent increases at the very early stages of nanocrystallization to values slightly above 1 to decrease down to $n$<0.5 as nanocrystallization progresses.

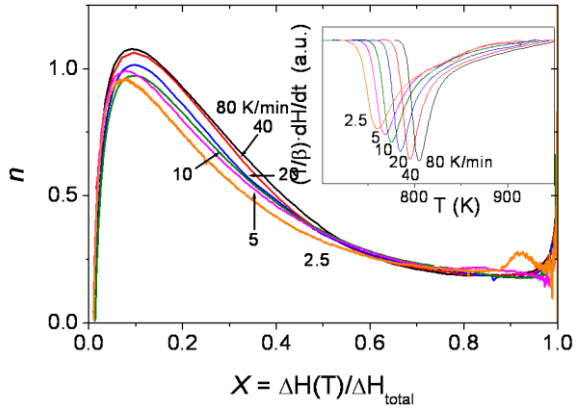


**Figure 3** $n(X)$ from non-isothemal DSC scans (inset).

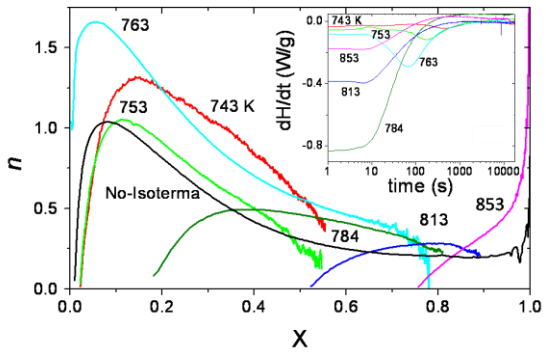


**Figure 4** $n(X)$ from isothermal DSC scans (inset). Non-isothermal values are also shown for comparison.

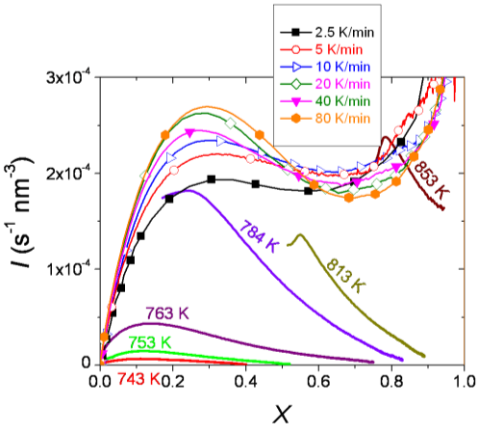

**Figure 5** $I(X)$ from isothermal and non-isothermal DSC scans.

The nucleation rate $I$ shows an enhancement of nucleation at low $X$ as $\beta$ increases and is strongly affected by the temperature in isothermal regimes, as expected for thermally activated processes. The different values are plotted in figure 5. For both regimes, the nucleation rate initially increases but, for isothermal one, $I(X)$ decreases as nanocrystallization progresses, whereas $I(X)$ remains almost constant for non-isothermal regimes. These dependencies can be explained from the two different nucleation mechanisms pointed above. At the early stages of nanocrystallization, there are not enough crystals for "in contact" nucleation mechanism to be significant. As the crystal population increases, this mechanism of nucleation is enhanced and $I(X)$ increases up to a maximum, after which $I(X)$ continuously decreases due to the progressive impoverishment of the amorphous matrix in Fe. This effect seems to be compensated in non-isothermal regimes due to the continuous increase of the temperature.

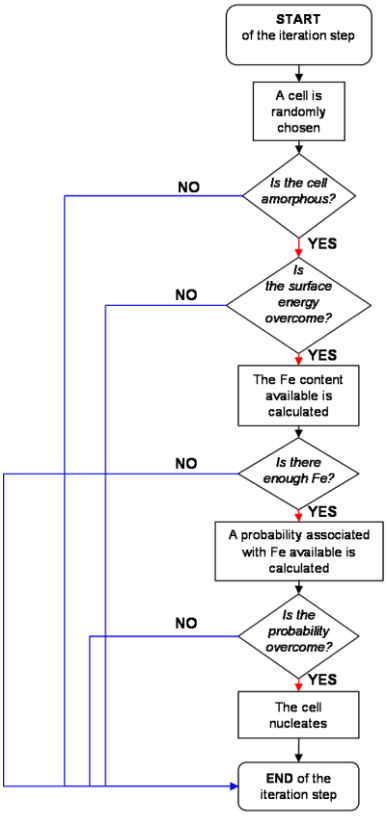


**Figure 6** Flow diagram of the simulation program.

### 4.2 Cellular automata simulations

The cellular automata simulation program used is detailed in Ref. [11]. In this simulation a three dimensional space is divided in cubic cells and the time is discretized in iteration steps. The stochastic character of nucleation is considered by randomly selecting a cell as candidate to develop a new crystalline nucleus. This cell will yield a nanocrystal only after fulfilling some deterministic and probabilistic requisites, which depend on the characteristic parameters of this cell and its neighborhood: volume available for nucleation, surface energy developed between the eventual new nucleus and its environment, and composition of the region where the nucleus would be formed. Figure 6 shows a flow diagram of the simulation program and table 1 summarizes the main parameters involved in the simulation. Figures 7 to 9 show the effect of changing these parameters on the kinetics of the modelled system.

**Table 1** Main parameters involved in the simulation.

| Parameter | Description |
|---|---|
| *vol* | Volume of the surrounding amorphous, in cell units, from which the forming nucleus can take Fe |

| | |
|---|---|
| σ | ~ excess surface energy of "isolated" nucleation with respect to "in contact" nucleation |
| $C_{Fe}$ | Fe content in volume vol |

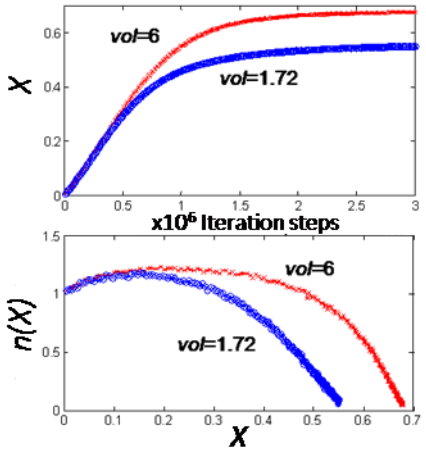


**Figure 7** $X(t)$ and $n(X)$ for two different values of the volume from which the new nucleus can take Fe: *vol*=6, complete 6 neighbor cells and *vol*=1.72, the smallest sphere in which the cubic crystal is contained. σ=0.5, composition $Fe_{60}Sol_{18}Exc_{22}$.

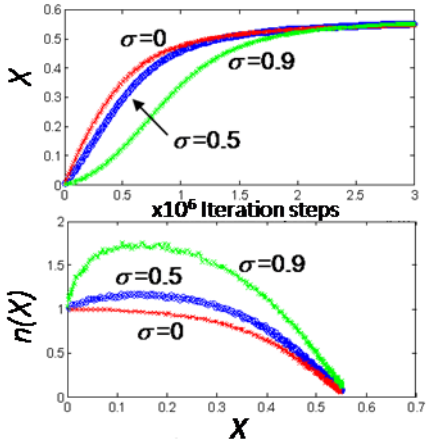


**Figure 8** $X(t)$ and $n(X)$ for *vol*=1.72, $Fe_{60}Sol_{18}Exc_{22}$ and three values of σ: σ=0 implies no surface energy advantage for "in contact" nucleation with respect to isolated one, σ=1 would prevent isolated nucleation.

An increase in the parameter *vol* implies an increase in the volume from which the forming nucleus can take the elements required. Thus it is related with the diffusion length and indirectly with the temperature. Therefore, as *vol* increases, kinetics becomes faster.

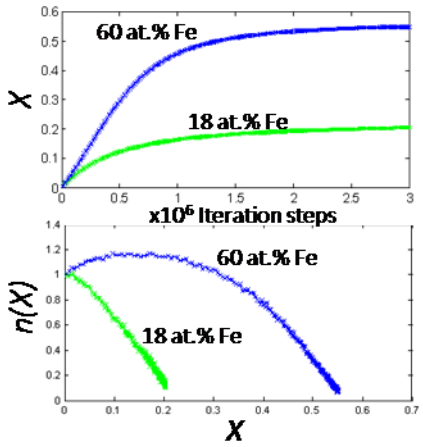


**Figure 9** $X(t)$ and $n(X)$ for two different values of the Fe concentration in $Fe_xCo_{78-x}Nb_6B_{16}$ simulated alloys. σ=0.5, *vol*=1.72.

If σ=0 there is no surface energy advantage for a nucleus to be formed in contact with an already formed crystal with respect to isolated nucleation. Therefore, Avrami exponent never rises above 1 as there is no enhancement in nucleation along the nanocrystallization process (which could resemble nanocrystallization of Cu containing alloys). As σ increases, the advantage of the "in contact" nucleation is enhanced with respect to the "isolated" one and the maximum of the Avrami exponent increases.

A general composition for Fe-based amorphous alloys able to nanocrystallize would be $Fe_xSol_yExc_{100-x-y}$; where Sol identifies the elements soluble in α-Fe (e.g. Co, Si, Ge), and Exc, those excluded from the crystalline phase and expelled out to the residual amorphous matrix (e.g. Nb, Zr, B). In the case of the alloys studied in the previous section, the composition of the crystals would be $Fe_{100-y}Co_y$ [12]. As Fe content of the alloy decreases, the amorphous surrounding crystallites becomes exhausted in this element faster, reducing the size of the agglomerates or even preventing their formation. Moreover, the final crystalline fraction decreases as there are fewer atoms able to form crystallites.

Figure 10 shows a plane of the simulated microstructure obtained after the same number of iterations for two different compositions. This plane would resemble a TEM image of 1 cell thickness and simulated and experimental images are compared in the figure. The absence of agglomeration, the smaller crystalline fraction and the exhaustion in Fe of the residual amorphous matrix in the richest Co alloy are clear whereas agglomerates and a larger crystalline fraction are evident in the Co poorest alloy.

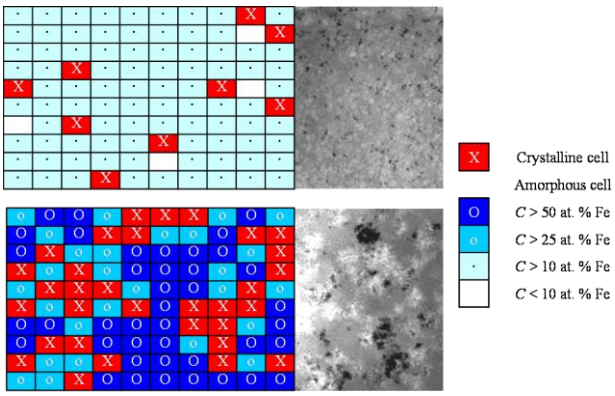


**Figure 10** Simulated (5 $10^5$ iterations) and experimental (5 h at 35 K below the corresponding onset of crystallization) images of two $Fe_{78-z}Co_zNb_6B_{16}$ alloys with z=60 (above) and 18 (below).

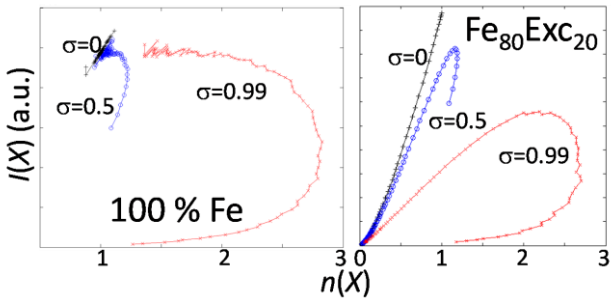


**Figure 11** $I(X)$ and $n(X)$ after simulation for a pure Fe alloy (left) and for a $Fe_{80}Exc_{20}$ alloy (right)

The slowing down of the nanocrystallization kinetics as the process progresses is generally ascribed to impingement of growth process, which is not applicable in the instantaneous growth approximation. Under the proposed approach, the slowing down of the kinetics is only due to two factors: progressive depletion of the amorphous matrix in the elements required to form a new nucleus and decrease of the number of nucleation sites. The first factor can be avoided if a pure Fe amorphous sample is simulated. Figure 11 (above) shows $n(X)$ and $I(X)$ for a pure Fe composition for different values of σ. For σ=0, nucleation rate does not change along the process and Avrami exponent is 1, in agreement with a constant nucleation rate. However, if σ>0, nucleation rate increases at the beginning as "in contact" mechanism can be relevant only after some nuclei are formed to supply such heterogeneous nucleation sites, which are more energetically favorable. Avrami exponent is in agreement with the behavior predicted by JMAK theory: $n$=1 for constant nucleation rate and $n$>1 for an increasing nucleation rate. However, if a non polymorphic transformation (composition changes from amorphous to crystalline phases) is considered with a strong advantage for "in contact" nucleation, the maximum in nucleation rate is clearly shifted to $n$>1 values as it can be observed in figure 11 (below). This indicates that for non polymorphic transformation, values of $n$>1 could correspond to a decreasing nucleation rate unlike predicted by JMAK theory.

## 5 Conclusions

In this work two approximations are applied to the nanocrystallization process of a FeCo-based alloy series.

Isokinetic approach allows us to obtain the local Avrami exponent as a function of the transformed fraction from a single non-isothermal scan and a raw estimation of the activation energy independently of the heating rate used.

Instantaneous growth approximation simplifies the nanocrystallization kinetics to nucleation phenomena. In order to explain the compositional dependencies of the nanocrystalline microstructures, two different nucleation mechanisms are described: in isolated regions and in contact with an already formed nanocrystal. The former mechanism occurs in a Fe richer region but the latter presents a lower surface energy between the new nucleus and the environment.

Cellular automata simulations agree with the described kinetics and microstructure. A speed up of nanocrystallization kinetics is observed when the mechanism of nucleation "in contact" is relevant (e.g. Cu free alloys with low Co content) and Avrami exponent initially rises above 1. As nanocrystallization progresses, kinetics is slowed down due to nucleation sites saturation and depletion of Fe in non-polymorphic transformation. In this transformation, which implies compositional changes from the amorphous to the forming nucleus, the value of $n$=1 is not obtained for the maximum nucleation rate achieved.

**Acknowledgements** This work was supported by the Spanish Ministry of Science and Innovation (MICINN) and EU FEDER (project MAT2007-65227) and the PAI of the Regional Government of Andalucía (project P06-FQM-01823). J.S. B. Acknowledges a research contract from Junta de Andalucía.

## References

[1] M. E. McHenry, M. A. Willard, D. E. Laughlin, Prog. Mater. Sci. 44, 291 (1999).
[2] M. T. Clavaguera-Mora, N. Clavaguera, D. Crespo, T. Pradell, Prog. Mat. Sci. 47, 559 (2002).
[3] W. A. Johnson, R. F. Mehl, Trans. Am. Inst. Mining Met. Engrs. 135, 416 (1939).
[4] M. Avrami, J. Chem. Phys. 9, 177 (1941).
[5] A. N. Kolmogorov, Bull. Acad. Sci. USSR, Phys. Ser. 1, 355 (1937).
[6] J. W. Christian, The Theory of Transformation in Metals and Alloys, Part 1 (Pergamon, Oxford, 1975), p. 542A.
[7] T. Tagami, S. I. Tanaka, J. Mat. Sci. 34, 355(1999)
[8] M. J. Starink, J. Mat. Sci. 36 4433 (2001).
[9] J. B. Austin, R. L. Rickett, Trans. Am. Inst. Mining Met. Engrs. 135, 396 (1939).
[10] J. S. Blázquez, M. Millán, C. F. Conde, A. Conde, Phil. Mag. 87, 4151 (2007).

[11] J. S. Blázquez, V. Franco, C. F. Conde, M. Millán, A. Conde, J. Non. Cryst. Solids 354, 3597 (2008)
[12] Y. Zhang, J. S. Blázquez, A. Conde, P. J. Warren, A. Cerezo, Mater. Sci. Eng. A 353, 158 (2003).
[13] J. S. Blázquez, C. F. Conde, A. Conde, Acta Mater. 53, 2305 (2005).